Far-field Environmental and Auto-Induced RF-EMF Human Absorption Simulations in Different Phantoms

Robin Wydaeghe[1], Bram Stroobandt[1], Mònica Guxens[2,] , Joe Wiart[3], Gabriella Tognola[4], Marta Parazzini[4], Wout Joseph[1]

[1]WAVES, Ghent University and IMEC, Department of Information Technology at Ghent University, Ghent, Belgium

[2]ISGlobal, Barcelona, Spain

[3]Télécom Paris, Institut Polytechnique de Paris, Palaiseau, France

[4]Institute of Electronics, Information Engineering and Telecommunications (IEIIT), Consiglio Nazionale delle Ricerche, Milan, Italy

BioEM 2025, Rennes, France.

Number of words in the summary: 146 of the 250 allowed.

Number of words in the main text: 2199 of the approximately 2500 allowed.

Summary

This study evaluates human exposure to radiofrequency electromagnetic fields (RF-EMF) in far-field conditions using numerical simulations. It distinguishes between environmental exposure (exposure from background RF fields) and auto-induced exposure (where 5G base stations direct beams toward users, increasing exposure levels). Simulations were conducted using a Finite-Difference Time-Domain (FDTD) method with four anatomical phantoms representing different ages and sexes. Exposure metrics include specific absorption rate (SAR) for frequencies below 6 GHz and surface-absorbed power density (S_{ab}) for frequencies above 6 GHz, following ICNIRP 2020 guidelines. Lower frequencies (<2 GHz) result in higher energy absorption, with children experiencing greater exposure due to smaller body sizes and different dielectric properties. Auto-induced exposure (5G beamforming) leads to 2–3 times higher exposure due to a focusing effect at the same frequency. Millimeter-wave exposure (above 24 GHz) is highly localized on the skin, with significantly reduced penetration compared to lower frequencies.

Introduction

Assessing human exposure to radiofrequency electromagnetic fields (RF-EMFs) requires precise quantification methods, as traditional questionnaire-based approaches lack accuracy in estimating absorbed exposure levels [1]. To overcome these limitations, numerical simulations provide an objective metric to estimate the specific absorption rate (SAR) and surface-absorbed power density (S_{ab}) across different frequencies, propagation conditions, and anatomical characteristics.

In particular for 5G, the Base Station (BS) is an active antenna instead of a passive antenna as in 4G wireless technology [2]. The antenna pattern is modulated in such a way to maximize signal locally near the User Equipment (UE). Therefore, the exposure is higher in an active-use scenario compared to a non-use scenario. When a 5G antenna beamforms toward an active user, the exposure is referred to as *auto-induced*. Conversely, for a non-user or a 4G active user, the exposure is referred to as *environmental*.

Existing literature either only concerns itself with environmental exposure [3], or the models do not account for the impact of next-generation wireless networks, particularly 5G, where beamforming introduces distinct exposure conditions. In 5G systems, exposure is categorized into environmental exposure—far-field exposure from background RF fields — and auto-induced exposure, where the base station actively directs beams toward a user, leading to localized RF energy concentration. Finally, for 6G, new frequency bands between 7 GHz and 12 GHz are considered (FR3), and also from 12 GHz to 24 GHz.

This study provides a comprehensive exposure assessment in the far-field region by computing numerical simulations of SAR and S_{ab} using four different anatomical phantoms that vary by age and sex in both the environmental and auto-induced cases. A systematic parametric study is conducted across multiple frequencies, considering both vertical and horizontal polarizations. The results provide insights into frequency-dependent absorption and the differential impact of 5G beamforming on exposure metrics.

Methods

Numerical simulations are performed using the Finite-Difference Time-Domain (FDTD) method. For this, the software Sim4Life from Zurich MedTech is used. The anatomical phantoms are provided by the IT'IS Foundation and their characteristics are listed in Table 1.

Table 1: Characteristics of the selected anatomical phantoms

Phantom	Sex	Age [years]	Height [m]	Weight [kg]
Duke	Male	34	1.77	70.2
Thelonious	Male	6	1.16	18.6
Ella	Female	26	1.63	57.3
Eartha	Female	8	1.36	29.9

The simulations were computed on an NVIDIA P100 GPU with 24 GB of virtual memory and a 40-core Intel E5-2630 CPU. The output of the simulations is the peak spatial SAR averaged over cubes of 10 g, as well as the whole-body SAR (not shown in this work), for frequencies below 6 GHz and the surface-absorbed power density averaged over 4 cm² for frequencies above 6 GHz, following the ICNIRP 2020 guidelines [4].

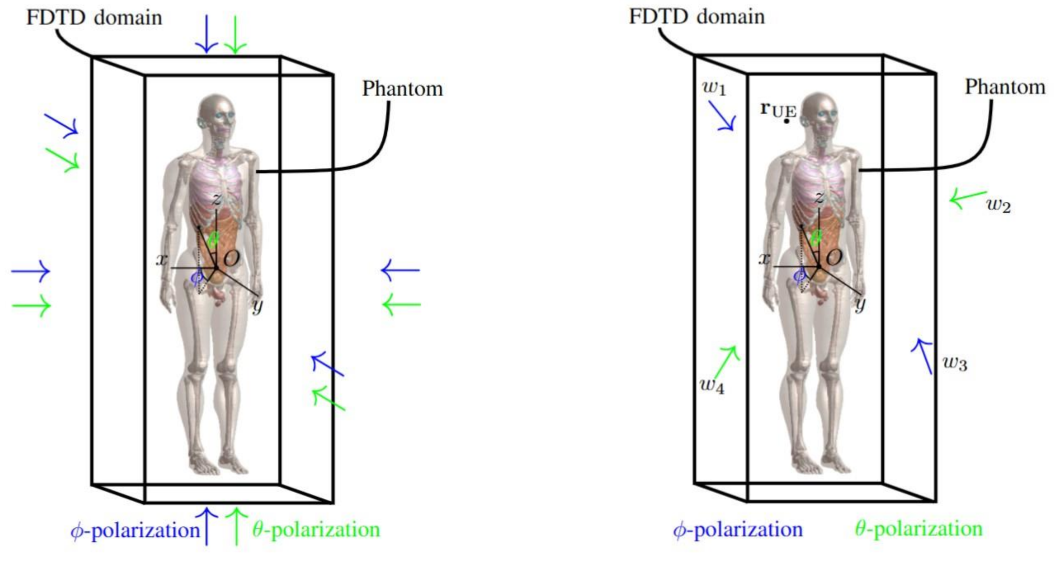

(a) Environmental exposure. All 12 Plane Waves (PWs) are shown, each corresponding to different simulations, having an amplitude of 1 V/m.

(b) Auto-induced exposure. Only 4 incident PWs are shown for brevity, with their weights w, to form one EMF around the phantom.

Figure 1: The setup for both environmental (a) and auto-induced (b) exposure scenarios. An anatomical phantom is placed in the FDTD simulation domain where the EMFs are computed using the TF/SF method.

Environmental far-field exposure

The simulation setup is shown in Fig. 1(a). With environmental exposure, we assume that the average EMFs originate from no particular direction. We can also assume the incident polarization to contribute equally in the vertical and horizontal directions. In order to reduce the number of simulations, only the six Cartesian directions $(+x, -x, +y, -y, +z, -z)$ aligned with the human body are simulated as incident waves in the far-field, each with either vertical or horizontal polarization. Therefore, 12 FDTD simulations are needed to compute the fields for one frequency. Due to the linearity of Maxwell's equations, the EMF from a combination of these incident waves can be summed—even when the amplitude of the waves is scaled. Therefore, we perform simulations with an incident amplitude of 1 V/m. The incident wave is a Plane Wave (PW) computed using the Total-Field/Scattered-Field (TF/SF) method.

Auto-induced far-field exposure

The simulation setup is shown in Fig. 1(b). With auto-induced exposure, the beam from the Base Station (BS) is attracted toward the user [5]. Therefore, the user induces the exposure onto themselves. To compute the exposure in this scenario, the propagation environment must be taken into account. A set of PWs is uniformly sampled in both elevation and azimuth every 5° in both polarizations. These are simulated with an amplitude of 1 V/m. A Multiple-Input Single-Output (MISO) channel from N transmitters to 1 receiver—the UE of the anatomical phantom under study—is considered. If $\mathbf{E}_{i,j,k}(\mathbf{r})$ denotes the steady-state electric field distribution resulting from an impinging PW with an amplitude of 1 V/m at an angle of arrival (θ_i, φ_j) and polarization k (vertical or horizontal), then the total field distribution $\mathbf{E}(\mathbf{r})$ is

$$\mathbf{E}(\mathbf{r}) = \Sigma_{i,j,k} w_{i,j,k} \, \mathbf{E}_{i,j,k}(\mathbf{r}) \, , \qquad (1)$$

due to the linearity of Maxwell's equations. The weights $w_{(i,j,k)}$ are determined such that the SNR at the UE is maximized, as is typical in, e.g., Maximum-Ratio Transmission (MRT) beamforming. As a proxy for the user device, the norm of the electric field is measured at the location of the UE, $\mathbf{r}_{\mathrm{UE}}$:

$$\max_{w} |\mathbf{E}(\mathbf{r}_{\mathrm{UE}})| \, . \qquad (2)$$

This can be achieved through standard MRT beamforming when considering a channel matrix to $\mathbf{r}_{\mathrm{UE}}$. Note that this represents a realistic worst-case scenario. In reality, each individual weight w cannot be controlled because an antenna element in a realistic MIMO antenna affects the amplitude and phase of multiple rays incident on the user. The total power of all weights is kept identical to the power from one incidence in the environmental case (1 V/m). Moreover, to compare with *non-functioning auto-induced exposure*, weights are also assigned randomly

$$w = A \exp(j \, \phi), \qquad (3)$$

where A is a random number obeying the aforementioned power constraint, and ϕ is a random number in $[0, 2\pi]$.

Results

The results of the numerical simulations for both environmental and auto-induced exposure are presented in this section. The exposure is quantified using the peak spatial SAR averaged over 10 g of tissue psSAR_{10g} for frequencies below 6~GHz and the surface-absorbed power density S_{ab} averaged over 4 cm^2 for frequencies above 6 GHz, following the ICNIRP 2020 guidelines. The results are computed for a list of frequencies shown in Table 2. Frequencies from 6G Frequency Range 3 (FR3) are also included.

Table 2: Frequencies to perform the simulations, with corresponding technology and exposure type (either Environmental (E) or Auto-Induced (AU)) and the exposure metric to quantify the EMFs in the body. FR2 and FR3 correspond to Frequency Range 2 and 3.

Frequency [GHz]	Technology	Exposure Type	Exposure Metric
0.450	Radio	E	SAR
0.700	5G NR	AU	SAR
0.835	2G GSM	E	SAR
1.450	Radio	E	SAR
2.140	4G LTE	E	SAR
2.450	Wi-Fi / Bluetooth	E	SAR
3.500	5G NR	AU	SAR
5.200	Wi-Fi	E	SAR
5.800	Wi-Fi	E	SAR
7.500	6G FR3	AU	S_{ab}
12.00	6G FR3	AU	S_{ab}
15.00	6G FR3	AU	S_{ab}
18.00	6G FR3	AU	S_{ab}
21.00	6G FR3	AU	S_{ab}
24.00	5G mmWave FR2	AU	S_{ab}
26.00	5G mmWave FR2	AU	S_{ab}

We will first discuss results in the environmental case, then the auto-induced case, and finally the result for 26 GHz.

Environmental far-field exposure

The computed $psSAR_{10g}$ as a function of frequency for environmental exposure (1 V/m PW) across the four anatomical phantoms is shown in Fig. 2. The sign and letter in the label determines the cartesian direction along which the plane wave travels; the superscript of the incidence label determines if the plane wave is polarized along the θ or ϕ direction from the phantom's center (see Fig. 1). Each subplot represents a different phantom (Duke, Ella, Thelonious, and Eartha), with multiple curves corresponding to different incident directions and polarizations of the plane wave.

A clear frequency dependence is observed, where the localized absorption generally decreases with increasing frequency. This trend is attributed to the decreasing penetration depth of electromagnetic waves at higher frequencies, resulting in reduced energy absorption within deeper tissues. Additionally, distinct differences are observed between child and adult phantoms, particularly at lower frequencies. For example, at 1.45 GHz, average deviations up to 74% and 83% are possible across sex and age, respectively.

To quantify these differences, Fig. 3(a) presents the exposure averaged across all incident directions for each phantom. The results indicate that child phantoms (Thelonious and Eartha) exhibit systematically higher $psSAR_{10g}$ values, between 4% and 55% compared to adult phantoms (Duke and Ella), especially below 2 GHz. This observation is consistent with existing literature and can be attributed to children's smaller body size and different dielectric properties, leading to increased energy absorption per unit mass.

Fig. 3(b) further examines the influence of the incident wave direction by averaging $psSAR_{10g}$ over all phantoms for each incidence direction. The results suggest that exposure is highly dependent on wave orientation, with the highest values observed for $+y^{\theta}$ and $-y^{\theta}$. The real-world variability in wave incidence is important when assessing RF exposure. The psSAR10g values decreases on average by 11.6 μW/kg/GHz.

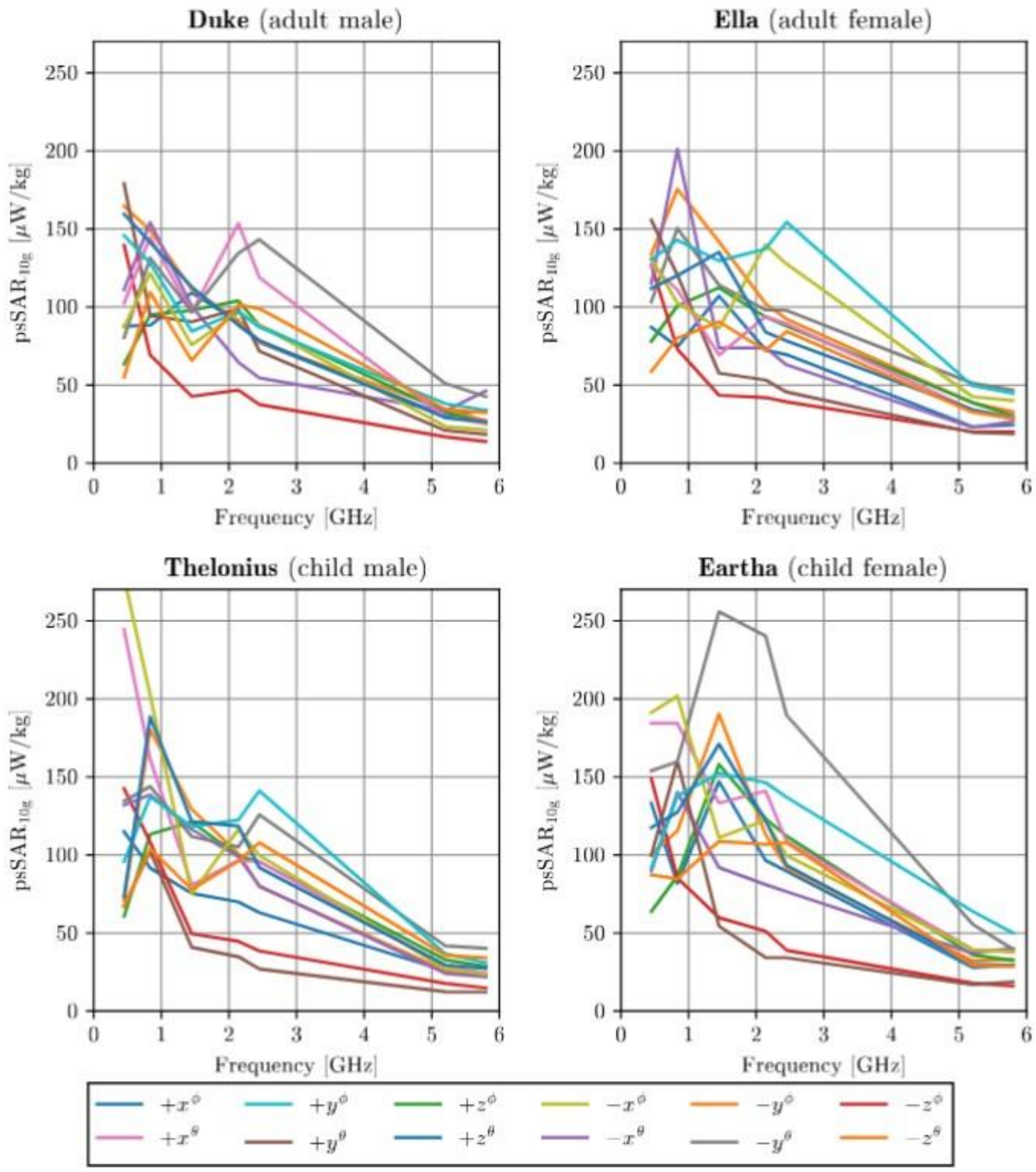

Figure 2: $psSAR_{10g}$ as a function of frequency for environmental exposure. The results are shown for four anatomical phantoms: Duke (adult male), Ella (adult female), Thelonious (child male), and Eartha (child female). Each colored curve represents a different incident wave direction and polarization.

Auto-induced far-field exposure

The results for auto-induced exposure, which corresponds to beamforming scenarios in 5G networks, show a significant increase in exposure results compared to non-functioning auto-induced exposure. For all phantoms, on average auto-induced exposure is approximately 2 to 3 times higher than the corresponding environmental exposure at 1 V/m in total at the same frequency. This aligns with results from literature [6]. The increase is attributed to the directional nature of the 5G base station beamforming, which concentrates electromagnetic energy toward the user. The differences between phantoms are still present, with children experiencing higher S_{ab} by 33% on average, but the relative increase due to beamforming remains consistent across all age groups.

Table 3: For all auto-induced frequencies, the increase of the fields compared to the non-functioning AU (Auto-Induced, where weights are scrambled randomly). The increase represents the effect of the focusing hotspot on the exposure.

Frequency [GHz]	Increase AU exposure compared to non-functioning AU exposure
0.700	1.7
3.500	1.9
7.500	2.3
12.00	2.4
15.00	2.8
18.00	2.6
21.00	2.9
24.00	3.1
26.00	3.0

Millimeter-wave exposure

At 24 and 26 GHz, the exposure is evaluated using the absorbed power density S_{ab} instead of $psSAR_{10g}$, as per ICNIRP 2020 guidelines [4]. In simulations, we observe a strong localization of energy absorption at the surface of the body, with significantly lower penetration compared to lower frequencies. This aligns with theoretical expectations, where millimeter-wave exposure primarily affects the superficial layers of the skin rather than deep tissues. This translates to a lower overall exposure metric, again decreasing with frequency. The polarization dependence seen in the lower frequencies is no longer present at these frequencies (within the margin of error), due to the wavelength being much smaller than the size of the phantom. At 24 GHz, the S_{ab} equalled 4.56 $\mu W/m^2$ and at 26 GHz, the S_{ab} equalled 2.23 $\mu W/m^2$.

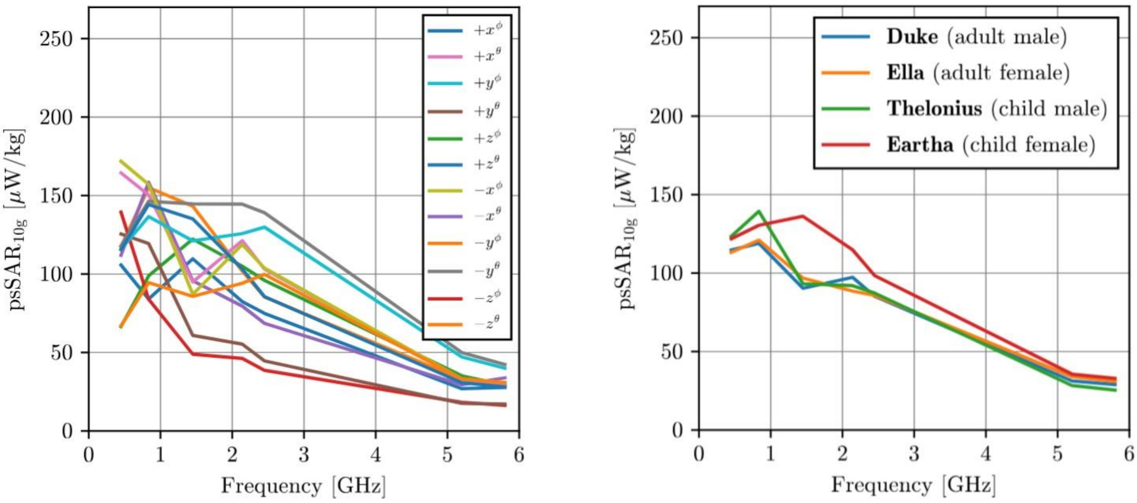

(a) Across all incident directions as a function of frequency for each phantom. Child phantoms exhibit higher exposure compared to adult phantoms, particularly at lower frequencies (<2 GHz).

(b) Across all phantoms as a function of frequency for different incidence directions. The highest exposure levels are observed for $\pm y^{\theta}$ and $\pm y^{\phi}$, indicating a polarization-dependent absorption effect.

Figure 3: psSAR10g for different phantoms and incident frequencies, averaged over either dimension.

Conclusion

This study systematically investigated far-field RF-EMF exposure through detailed FDTD simulations of both environmental and auto-induced scenarios over a broad frequency spectrum. Our findings demonstrate a clear inverse relationship between frequency and psSAR, with lower frequencies resulting in higher energy absorption and pediatric phantoms exhibiting greater exposure than adult models, especially below 2 GHz. Auto-induced exposure scenarios, emblematic of 5G beamforming, resulted in significantly elevated psSAR values, roughly 2–3 times those observed under environmental conditions. In the millimeter-wave domain (26 GHz), energy absorption was predominantly confined to the skin's superficial layers, in line with literature. Future work should extend these analyses to near-field conditions and include experimental validations to further refine risk assessments and to embed the results in a transfer function matrix as part of an objective metric in epidemiological studies.

Acknowledgments

This project has received funding from the European Union's Horizon Europe research and innovation programme under grant agreement No 101057262 (GOLIAT). Views and opinions expressed are however those of the authors only and do not necessarily reflect those of the European Union or the Health and Digital Executive Agency. Neither the European Union nor the granting authority can be held responsible for them.

References

[1] L. van Wel *et al.*, "Radio-frequency electromagnetic field exposure and contribution of sources in the general population: an organ-specific integrative exposure assessment," *J. Expo. Sci. Environ. Epidemiol.*, vol. 31, no. 6, pp. 999–1007, 2021.

[2] R. Wydaeghe *et al.*, "Realistic Human Exposure at 3.5 GHz and 28 GHz for Distributed and Collocated MaMIMO in Indoor Environments Using Hybrid Ray-Tracing and FDTD," *IEEE Access*, vol. 10, pp. 130996-131004, 2022.

[3] G. Vermeeren, W. Joseph, C. Olivier and L. Martens, "Statistical multi-path exposure of a human in a realistic electromagnetic environment," *Health Physics*, vol. 96, no. 6, pp. 629-636, 2009.

[4] ICNIRP (International Commission on Non-Ionizing Radiation Protection), "Guidelines for limiting exposure to electromagnetic fields (100 kHz to 300 GHz)," *Health Physics*, vol. 118, no. 5, pp. 483-524, 2020.

[5] I. Nasim and S. Kim, "Human exposure to RF fields in 5G downlink," *IEEE International Symposium on Antennas and Propagation*, 2019.

[6] D. Plets et al., "Time-averaged exposure assessment for massive MIMO 5G NR base stations with beamforming and its impact on EMF exposure guidelines," *IEEE Access*, vol. 9, pp. 39102-39111, 2021.